Evolution of Small Molecule Content and Morphology with Dip-Coating Rate in Supramolecular PS–P4VP Thin Films

ARTICLE *in* MACROMOLECULES · OCTOBER 2012

Impact Factor: 5.8 · DOI: 10.1021/ma301383v

4 AUTHORS, INCLUDING:

Sébastien Roland
MINES ParisTech
8 PUBLICATIONS **51** CITATIONS

SEE PROFILE

Macromolecules

Article

pubs.acs.org/Macromolecules

Evolution of Small Molecule Content and Morphology with Dip-Coating Rate in Supramolecular PS−P4VP Thin Films

Sébastien Roland, Christian Pellerin,* C. Geraldine Bazuin,* and Robert E. Prud'homme*

Département de chimie, Centre de recherche sur les matériaux auto-assemblés (CRMAA/CSACS), Université de Montréal, C.P. 6128 succursale Centre-ville, Montréal (QC), Canada H3C 3J7

Supporting Information

ABSTRACT: In dip-coated thin films of supramolecular block copolymers where a small molecule (SM) preferentially interacts with one of the blocks, an important issue is whether or not the SM content in the films is the same as that in the dip-coating solution. Here, we quantitatively determined the SM content, using infrared spectroscopy in the attenuated total reflection mode (IR-ATR), in films of poly(styrene-*b*-4-vinylpyridine) (PS−P4VP) dip-coated from THF solutions containing naphthol (NOH) and naphthoic acid (NCOOH). Dip-coating was effected at very slow rates (0.5−6 mm/min), i.e., in the recently described "capillarity regime", where film thickness decreases with rate. It was found that, for both SMs, the SM/VP ratios in the films are the same under given conditions and evolve identically with dip-coating rate, starting from much less than, and then increasing toward, the SM/VP solution ratio. This behavior was related to THF being a hydrogen-bond competitor and to consequent diffusion of the SM back into solution during the capillarity-dominated dip-coating process. The increase in the SM/VP ratio correlates with a morphology evolution from spherical to (in-plane) cylindrical to lamellar in the NCOOH-containing films. The more limited morphological evolution in the films containing NOH, which forms a weaker H-bond with VP than NCOOH, was attributed mainly to greater partitioning of NOH in the PS phase.

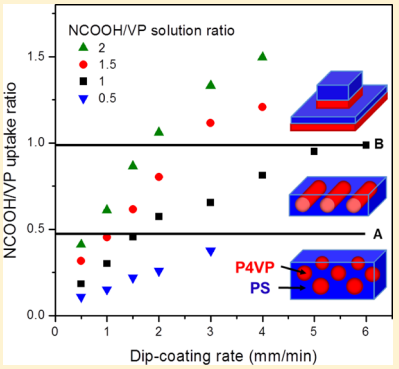

INTRODUCTION

Diblock copolymers are commonly used to create patterned surfaces at the nanometer scale in view of their growing interest for applications related to electronics,[1] optoelectronics,[2] biosensors,[3] nanolithography,[4] and nanoreactors.[5] The nanophase separation induced by the immiscibility of the two blocks leads to characteristic morphologies that can be tuned by changing key parameters such as the Flory−Huggins interaction parameter between the two blocks, their degree of polymerization, and the relative block fraction.[6] In the case of block copolymer thin films, interfacial interactions, which often favor wetting of surfaces by one of the blocks, and film thickness, especially in relation to the natural periodicity of the block copolymer, also influence the film morphology.[7−10] In most studies leading to this understanding, block copolymer thin films were prepared by spin-coating, where film thickness is controlled by solution concentration and spin-coating parameters, generally followed by annealing. Dip-coating, an important industrial technique, is an alternative method for obtaining thin films. It has been used only occasionally to date for block copolymer studies and can have particular consequences for supramolecular films, as will be shown here.

"Supramolecular control" of block copolymer morphology is based on utilizing preferential interactions of functional small molecules (SMs) with one of the blocks.[11−15] In a series of articles, Stamm and co-workers employed HABA [2-(4′-hydroxybenzeneazo)benzoic acid] to influence the morphology of poly(styrene-*b*-4-vinylpyridine) (PS−P4VP) diblock copolymer thin films through hydrogen bonding of HABA to P4VP.[11,13,16−18] They showed that dip-coating from chloroform and dioxane solutions leads to horizontal and vertical cylindrical morphologies, respectively, where the cylinders are the P4VP/HABA phase.[17] Furthermore, increasing the amount of HABA in the dip-coating solution switches the morphology of the dip-coated thin film in dioxane from vertical to horizontal cylinders, which was related to increased preferential swelling of the P4VP phase and hence to the pathway taken in the phase diagram during film drying.[18] In other examples, ten Brinke and co-workers[19,20] and Tung et al.[21] blended PDP (3-*n*-pentadecylphenol) with PS−P4VP, in these cases in spin-coated thin films, and, in some cases, were able to obtain morphological order on two length scales, involving the block copolymer and PDP, respectively.

In our group, we have been investigating PS−P4VP films dip-coated from THF solutions containing other hydrogen-bonding small molecules (SMs), namely, 1,5-dihydroxynaphthalene (DHN)[14] as well as naphthol (NOH) and naphthoic acid (NCOOH).[22,23] In comparing films prepared from NOH- and NCOOH-containing solutions, we found that the film morphology depends on the dip-coating rate and that its

Received: July 5, 2012
Revised: September 6, 2012
Published: September 19, 2012

evolution with dip-coating rate is different for the two types of solutions.[22a,23] At the lowest rates used, both SMs lead to a surface pattern of quasi-hexagonally ordered dots, reflecting spherical morphology and related to the micellar THF solutions.[22a] However, as dip-coating rate is increased, a stripe (fingerprint) morphology, reflecting in-plane cylinders, appears in some conditions, favored in particular by NCOOH more than NOH, by higher polymer concentration in solution, and by higher SM:VP ratio in solution.[22a] These investigations were performed at slow dip-coating rates, where the film thickness decreases with increase in rate.

To understand these trends, a crucial question that is specific to dip-coated films of supramolecular block copolymers is whether or not the SM/VP ratio in the film is the same as in solution. If not, is the amount in the film dependent on the choice of SM, on the solvent used, or on dip-coating parameters, to thereby influence the final film morphology? For example, Huang et al.[24] showed by NMR that the small molecule PDP and the P4VP block exhibit different degrees of complexation in solution depending on the solvent and that this influences the morphology obtained in the (spin-coated) films. They distinguished solvents whose molecular structure includes an oxygen atom, which, as a hydrogen-bond acceptor, competes with the pyridine ring for complexation with the small molecule, from solvents without an oxygen atom, and showed that these two types of solvents influence cylindrical orientation differently.

In this paper, we present a method to quantify the amount of small molecule in the dip-coated films, using attenuated total reflection infrared (ATR-IR) spectroscopy. With this tool, the SM/VP molar ratios in the dip-coated films of a PS−P4VP diblock copolymer containing NOH and NCOOH are compared as a function of dip-coating rate and of the SM/VP molar ratio in solution. The results are correlated with the evolution in film surface morphology as determined by atomic force microscopy (AFM) and with the change in film thickness, which is discussed in the light of the recently described "capillarity" vs "draining" regimes for dip-coated films.[23,25,26]

Scheme 1. Molecular Structure of the Two Small Molecules Used

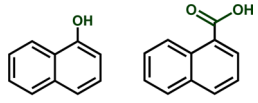

NOH NCOOH

EXPERIMENTAL SECTION

Materials. A PS−P4VP diblock copolymer, with M_n(PS) = 41.5 kg/mol and M_n(P4VP) = 17.5 kg/mol (29.7 mol % P4VP), was purchased from Polymer Source and used as received. PS (M_w = 110 kg/mol; PDI < 1.05) and P4VP (M_w = 60 kg/mol) homopolymers were obtained from Pressure Chemical Company and Sigma-Aldrich, respectively. 1-Naphthol (NOH, >99%), 1-naphthoic acid (NCOOH, 99.8%), and tetrahydrofuran (THF, 99.99%) were purchased from Sigma-Aldrich, Fluka, and VWR, respectively, and used as received. Silicon wafers ({1,0,0}) were purchased from University Wafer (Pittsburgh). Rectangular shards, cut to appropriate dimensions (approximately 10 × 5 mm^2 for dip-coated films and 10 × 10 mm^2 for solvent-cast films), were cleaned by immersion in THF for 5 min in an ultrasonic bath, wiped with Kimwipes tissue, and dried under nitrogen flow. Out of precaution, they were additionally cleaned by immersion in a piranha solution [7/3 v/v concentrated H_2SO_4 and H_2O_2 (30 wt %)] at 90 °C for 1 h, thoroughly rinsed with Milli-Q water, and dried under nitrogen flow, although this step was not observed to make a significant difference for the results.

Film Preparation for ATR-IR and AFM Studies. Dip-coating solutions of 5 mg/mL (with respect to the copolymer) were prepared by dissolving 25 mg of PS−P4VP and the required amount of SM for the SM/VP molar ratio desired in 5 mL of THF. The solutions were stirred overnight in closed vials on a heating plate at ca. 40 °C (in early work, 60−70 °C was used, with no detectable difference in the morphologies), were left to cool to ambient temperature, and then were filtered successively through 0.45 and 0.2 μm PTFE filters (VWR). All dip-coating experiments were carried out under ambient conditions (21 °C, variable humidity); no significant differences were found in films prepared under high or low ambient humidity conditions. The silicon substrates were vertically immersed in the solutions at a rate of 5 mm/min, followed by a 30 s pause, and then were vertically withdrawn from the solutions at a controlled rate using a KSV 3000 Langmuir film balance. The films were left to dry in covered containers overnight.

For calibration plots, 5 mg/mL solutions were prepared by dissolving 25 mg of block copolymer in 5 mL of chloroform at the desired SM/VP molar ratio. After complete dissolution on a stirring plate, a droplet of the solution was cast to completely cover the silicon shard. Chloroform was used because it allowed the formation of homogeneous films during solvent evaporation, in contrast to THF, for which heterogeneities on the sample surface (observed by the naked eye) degraded the infrared spectra.

Fourier Transform Attenuated Total Reflection Infrared Spectroscopy (ATR-IR). ATR infrared spectra, obtained from an accumulation of 256 interferograms at a resolution of 4 cm^{-1}, were recorded with a Tensor 27 Bruker Optics spectrometer equipped with a MCT (mercury cadmium telluride) detector and a Harrick Seagull accessory. A hemispherical Ge ATR crystal was used with p-polarized radiation at a 65° incident angle.

Atomic Force Microscopy (AFM). AFM images were obtained in tapping mode using a Multimode microscope controlled by a Nanoscope V controller (Bruker), operated under an ambient atmosphere. The tips (Arrow-NCR, Al coated, spring constant 42 N/m, oscillation frequency ca. 285 kHz) were obtained from Nanoworld. Film thicknesses were determined from AFM images of scratches made with a scalpel.

Differential Scanning Calorimetry (DSC). Temperature-modulated scanning calorimetry was performed using a DSC Q1000 from TA Instruments. All samples were heated at a rate of 5 °C/min, with an oscillation amplitude of 1 °C and an amplitude period of 40 s. Data were taken from the second heating thermogram using the inflection point method to determine the T_g. The blends were prepared by dissolving the SM and homopolymer (PS and P4VP) in $CHCl_3$ in the desired ratio (in steps of 5 wt %, up to 30 wt %) and then solvent casting, followed by drying for 3 h at ambient temperature in a vacuum oven. $CHCl_3$ instead of THF was chosen because P4VP is not soluble in THF and also because $CHCl_3$ can be removed more easily than THF from the solvent-cast films without leading to undesired SM evaporation. Complete evaporation of $CHCl_3$ appeared assured by the fact that the pure homopolymers prepared in the same way as the blends showed the same T_g as the untreated homopolymers (106 and 152 °C for PS and P4VP, respectively).

RESULTS AND DISCUSSION

The influence of the type of SM on the morphology of film dip-coated from 5 mg/mL PS−P4VP THF solutions containing equimolar SM relative to VP, illustrated in Figure 1, concords with our previous findings.[22a] The dot morphology, reflecting P4VP/SM spheres in a PS matrix, is observed in films of PS−P4VP/NOH (NOH/VP = 1.0) for all three dip-coating rates shown (Figure 1a$_1$−c$_1$). In contrast, in films of PS−P4VP/NCOOH (NCOOH/VP = 1.0), the dot morphology is observed for dip-coating at 1 mm/min (Figure 1a$_2$) and a

dx.doi.org/10.1021/ma301383v | Macromolecules 2012, 45, 7964−7972

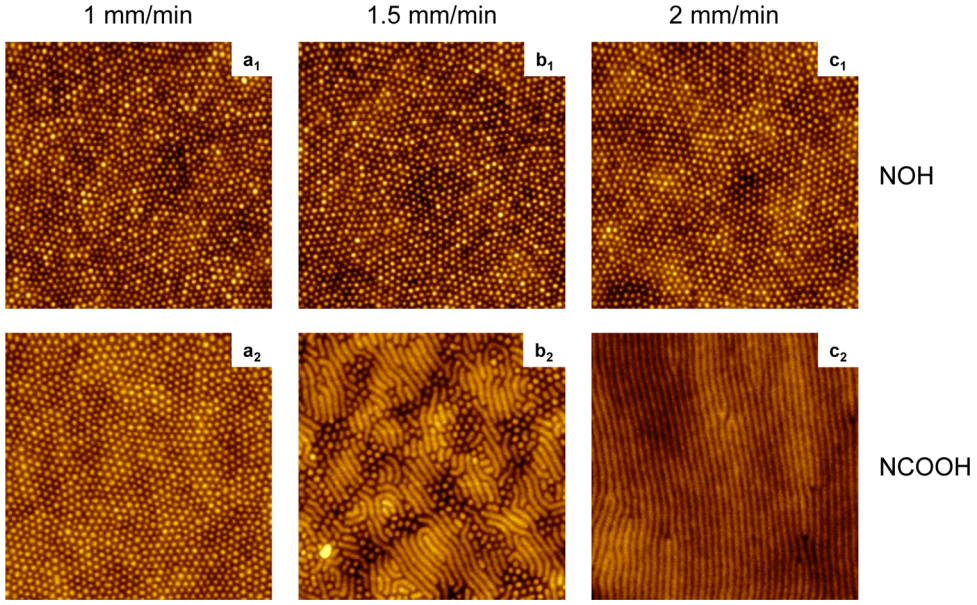

Figure 1. AFM topographic images (2×2 μm^2, z = 10 nm) of PS−P4VP diblock copolymer films dip-coated at the rates indicated from THF solutions containing SM═NOH or NCOOH at equimolar SM/VP ratios.

stripe (fingerprint) morphology, representing in-plane cylinders of P4VP/SM, is observed for dip-coating at 2 mm/min (Figure $1c_2$). A transition between the two morphologies occurs at the intermediate dip-coating rate of 1.5 mm/min (Figure $1b_2$). It was verified by light scattering that there is no significant difference in the hydrodynamic radii and the radii of gyration of the NOH- versus the NCOOH-containing (or even SM-free) PS−P4VP solutions in THF and therefore in the shape and size of the micelles that are characteristic of these solutions.[22a] In addition, the average film thickness was found to decrease monotonically with increase in dip-coating rate, from ca. 150 nm at a rate of 0.1 mm/min to a minimum of ca. 10 nm at the highest rates investigated (5−8 mm/min).[22a] For these thinnest films, the surface morphology appears featureless or predominantly featureless, reflecting a "brush" layer of substrate-wetting P4VP covered by PS that minimizes the interfacial energy with air.[22a,27] The decrease in film thickness with dip-coating rate was correlated[22a] with the "capillarity regime" described recently by Grosso and co-workers for dip-coated sol−gel films,[25,26] as will be discussed further below.

It was verified previously by transmission infrared spectroscopy of thick films cast from THF solutions that NOH and NCOOH hydrogen bond to the pyridine block.[22a] To recapitulate briefly, the usual band shifts associated in previous literature with OH and COOH H-bond interactions with pyridine were observed in the solvent-cast films (equimolar SM/VP). The quasi-disappearance of the 993 cm^{-1} free pyridine band indicates that the SM−VP H-bond interactions in these films are close to complete. It is also known from the literature that the COOH moiety forms a stronger H-bond with VP than the OH moiety (considered to be strong and intermediate strength, respectively),[29] as evidenced by two broad bands at 2500 and 1950 cm^{-1} for COOH−VP interactions that are not present for OH−VP interactions.[22a] This is supported by the somewhat higher wavenumbers to which the 993 and 1598 cm^{-1} free VP bands are shifted by H-bonding in the NCOOH-containing films (to 1013 and 1605 cm^{-1}, respectively, for equimolar SM:VP) compared to the NOH-containing films (to 1007 and 1603 cm^{-1}, respectively). It may be added that the quasi-completeness of SM−VP H-bonding in the dried films is favored by its greater strength compared to self-hydrogen bonding (OH−OH and COOH−COOH, respectively)[29c] as well as by the combinatorial entropic contribution to the free energy of mixing (polymer−SM interactions being more favorable than SM−SM interactions).

In the present study, infrared (IR) spectroscopy investigations in the attenuated total reflection (ATR) mode were carried out on dip-coated films. Figure 2 shows representative ATR-IR spectra of such films containing the two SMs, compared with the spectra of the separate components. ATR-IR spectroscopy is a surface technique, and therefore, to ensure that the entire film thickness is being characterized, the depth of penetration should exceed the film thickness. Since the films are dip-coated onto silicon substrates, this requirement is verified by observation of the very broad Si−O−Si stretching band near 1200 cm^{-1} (Figure 2b). This band is present in the spectra of the SM-containing films shown in Figure 2d,g, as it is in all of the dip-coated films analyzed, including the thickest ones.

By comparing the PS−P4VP/SM spectra with those of the components alone (Figure 2a,c,f), isolated bands with no significant overlap among the different components and free of H-bond effects—therefore, useful for quantitative analysis—can be identified, notably, 1493, 1510, and 1387 cm^{-1} for PS−P4VP, NCOOH, and NOH, respectively. These bands, listed in Table 1, have constant absorption frequencies independent of film composition, indicating that they are not affected by the hydrogen-bonding interactions. This is in contrast to, for example, the 1600 cm^{-1} composite band, where H-bonding shifts the P4VP component of the band to higher wavenumbers.[22a,28,29] Thus, the 1493 cm^{-1} PS−P4VP band will be used as the reference band for normalization of the spectra, and the two SM bands will be used to quantify the amount of SM in the films.

To make quantitative measurements of the SM/VP ratio in the films, ATR-IR calibration plots were prepared using samples that were solvent-cast on silicon wafers from solutions

dx.doi.org/10.1021/ma301383v | Macromolecules 2012, 45, 7964−7972

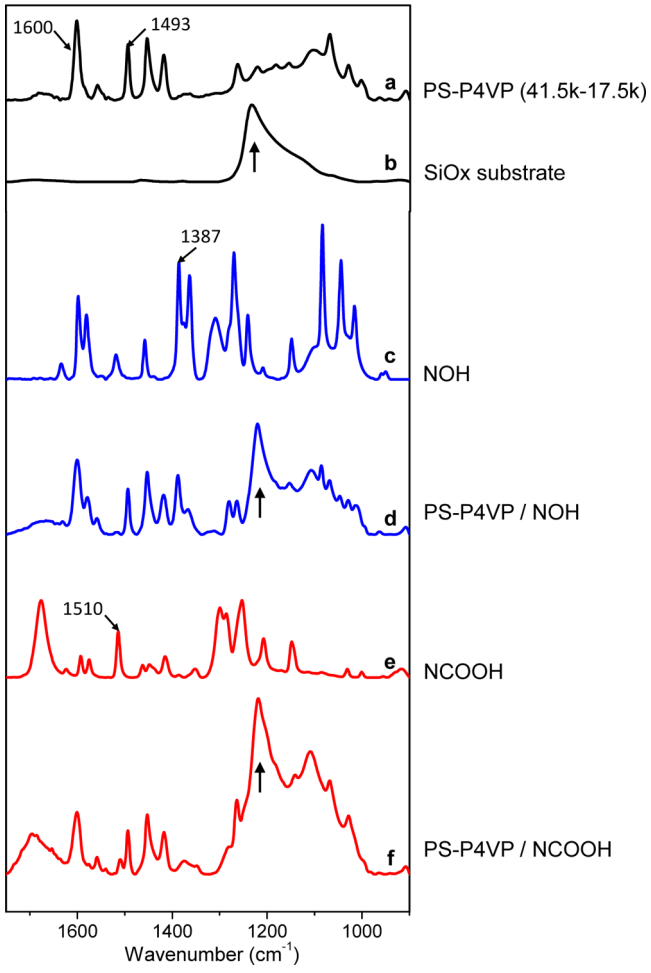

Figure 2. ATR-IR spectra of (a) solvent-cast PS–P4VP, (b) bare silicon wafer (substrate), (c) naphthol (powder), (d) PS–P4VP film dip-coated at 2 mm/min from a NOH-containing THF solution, (e) naphthoic acid (powder), and (f) PS–P4VP film dip-coated at 2 mm/min from a NCOOH-containing THF solution; (d) and (f) are for equimolar SM/VP solutions. Arrows indicate the Si–O–Si stretching band from the oxide layer on the silicon substrate.

Table 1. Principal Infrared Vibration Frequencies of the PS–P4VP Block Copolymer[30,31] and the Small Molecules (NOH and NCOOH)[32] Referred to in the Text (All Are Ring Stretching Modes)

wavenumber (cm^{-1})	attribution
1600	PS, P4VP, NOH, NCOOH
1510	NCOOH
1493	PS, P4VP
1415	P4VP
1387	NOH
993	P4VP

of several SM/VP molar ratios (0, 0.25, 0.5, 0.75, and 1.0), which necessarily give the same SM:VP molar ratios in the films. The plots are shown in Figure 3, where the ratio of the height of the SM band (1387 and 1510 cm^{-1} for NCOOH and NOH, respectively) to the height of the PS–P4VP band at 1493 cm^{-1}, using the baselines indicated in Figure 4 and applying band fitting in the case of NCOOH. The data points in Figure 3 show well-behaved linear relationships obeying the Beer–Lambert law.

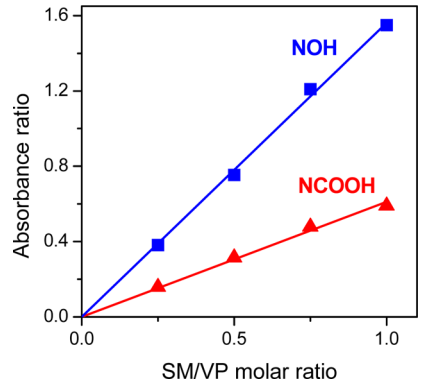

Figure 3. Calibration plots determined from ATR-IR spectra of solvent-cast PS–P4VP films containing known concentrations of NOH and NCOOH. Absorbance ratios are determined using the NOH band at 1387 cm^{-1} and the NCOOH band at 1510 cm^{-1} relative to the PS–P4VP band at 1493 cm^{-1}. The linear plots are least-squares fits of the data points forced through the origin.

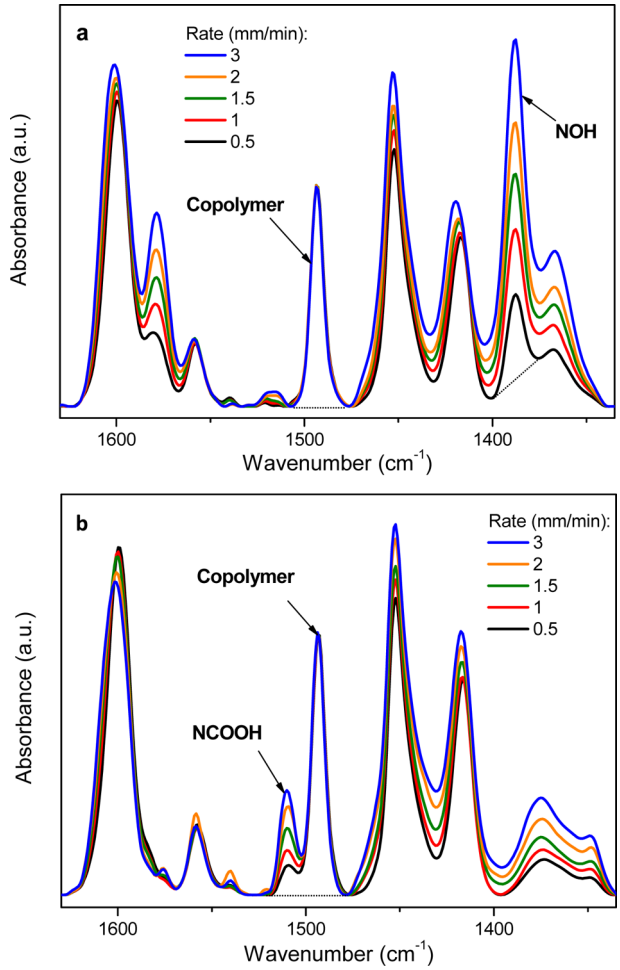

Figure 4. ATR-IR spectra of PS–P4VP films dip-coated at the withdrawal rates indicated from THF solutions containing (a) NOH and (b) NCOOH in equimolar SM/VP ratio. The spectra are normalized to the copolymer band at 1493 cm^{-1}. Baselines are indicated for the bands used for quantitative analysis.

Figure 4 displays the ATR-IR spectra of dip-coated films obtained at various dip-coating rates from equimolar SM/VP solutions. The spectra are normalized to the copolymer band at

dx.doi.org/10.1021/ma301383v | Macromolecules 2012, 45, 7964–7972

1493 cm^{-1}, thus highlighting the change in relative intensity of the SM bands. Clearly, the intensity of the latter increases with dip-coating rate, indicating that the SM/VP ratio in the films ("uptake ratio") increases with dip-coating rate. In parallel, there is a gradual shift of the band near 1600 cm^{-1} from 1598 to 1601 cm^{-1} for NOH and to 1602 cm^{-1} for NCOOH with increase in SM/VP ratio, reflecting an increase in SM hydrogen bonding to VP that shifts the pyridine contribution of this composite band to slightly higher wavenumbers.[28,29] The shift causes a broadening of this band and thus accounts for its decrease in intensity (constant total area) with NCOOH/VP ratio. In contrast, the intensity increases with NOH/VP ratio due to the overlap with a relatively intense NOH band at 1598 cm^{-1} (see Figure 2c,e).

Using the bands at 1387 and 1510 cm^{-1} for NOH and NCOOH, respectively, along with the calibration curves, the quantitative SM/VP uptake ratios in the films dip-coated from equimolar solutions are plotted as a function of dip-coating rate in Figure 5. It can be observed that the increase in SM/VP uptake ratio is quasi-linear at low dip-coating rates up to ca. 2–3 mm/min, after which it rises more slowly, tending toward the solution SM/VP ratio. It is noteworthy that the uptake ratios for the two SMs at any given dip-coating rate are very similar. Thus, it can be concluded that the morphological differences between NOH- and NCOOH-containing films, as illustrated in Figure 1, cannot be accounted for by a difference in the SM/VP uptake ratio.

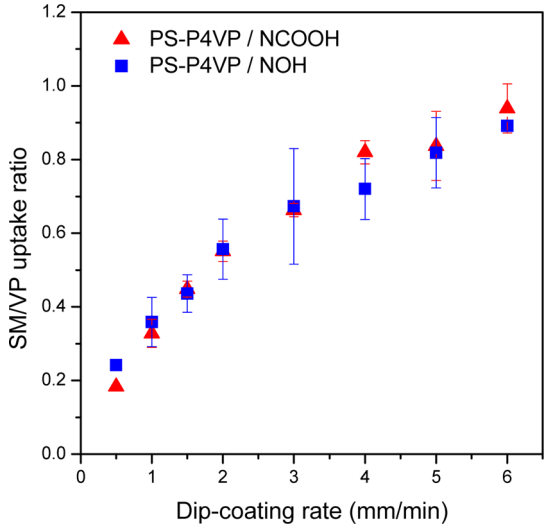

Figure 5. SM/VP uptake ratio as a function of dip-coating rate in PS–P4VP films dip-coated from THF solutions containing NCOOH and NOH in equimolar SM/VP ratio.

Because it is the NCOOH-containing films that show greater richness in morphological evolution as a function of dip-coating rate in the conditions studied, further investigations concentrate on these films. Figure 6 shows the NCOOH/VP uptake ratio as a function of dip-coating rate for films dip-coated from solutions of four different NCOOH/VP molar ratios. They all show the same trend, namely a quasi-linear increase in NCOOH/VP uptake ratio with dip-coating rate up to about 2–3 mm/min that then more slowly tends toward a plateau corresponding to the solution ratio. When the uptake ratios in Figure 6 are normalized to the solution ratio, they collapse to a single curve (Figure 7). This indicates that the uptake ratio is directly proportional to the solution ratio for a given dip-coating rate.

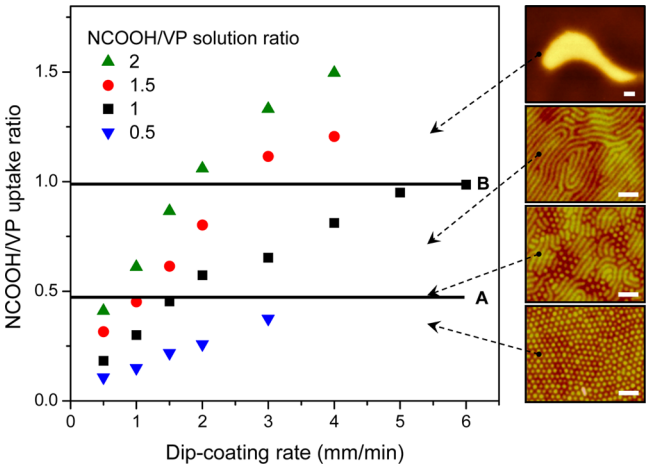

Figure 6. NCOOH/VP uptake ratio in PS–P4VP films as a function of dip-coating rate from solutions containing the NCOOH/VP molar ratios indicated. The film morphologies observed by the representative AFM height images shown are dots (spherical) below line A, stripes (in-plane cylindrical) between lines A and B, and islands and holes (in-plane lamellar) above line B. A transition morphology of dots and stripes is observed in the vicinity of line A. AFM scale bars = 200 nm (500 nm for the topmost image).

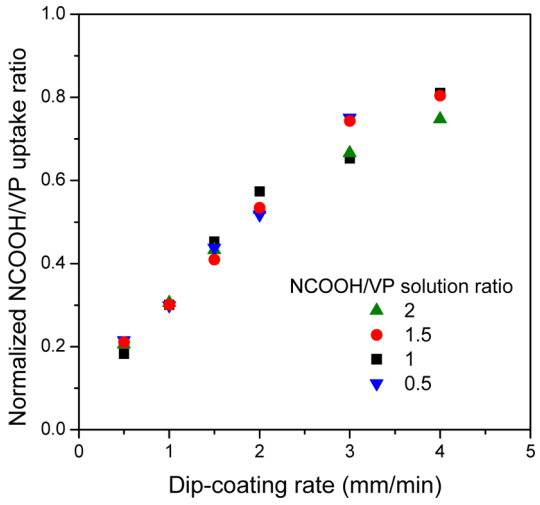

Figure 7. NCOOH/VP uptake ratios as a function of dip-coating rate for the PS–P4VP films of Figure 6 normalized by the NCOOH/VP solution ratios indicated.

The film morphologies observed by AFM are also indicated in Figure 6. This figure can be divided into three main morphological areas separated by the horizontal lines, A and B, and can thus be viewed as a pseudophase diagram. Below line A, only the dot (spherical[22a]) morphology and never the stripe morphology is observed. Between lines A and B, the opposite—i.e., the stripe (in-plane cylindrical[22a]) morphology and never the dot morphology (but accompanied by featureless regions for dip-coating rates of 3 mm/min and above; see below in connection with film thickness variation)—is observed. A transitional morphology, i.e., the presence of both dots and short stripes, is observed in the vicinity of line A. Above line B, where the solution ratio exceeds equimolar SM/

dx.doi.org/10.1021/ma301383v | Macromolecules 2012, 45, 7964–7972

VP, the morphology resembles "islands and holes", where the step height is ca. 25 nm. This morphology is typical of lamellar organization parallel to the substrate in the form of terraces due to the incommensurability between the average film thickness and the natural block copolymer periodicity.[9,10]

The fact that lines A and B separating the morphology zones in Figure 6 are horizontal suggests that the film morphology is controlled by the NCOOH/VP uptake ratio in these films and only indirectly by the dip-coating rate through its effect on that ratio. This can be understood, at least in part, by considering the degree of swelling of the P4VP phase by NCOOH, relative to the morphology in pure PS−P4VP dip-coated from SM-free THF solutions. The SM-free films show the dot (spherical) morphology in the whole range of dip-coating rates studied here, attributed to the deposition of solution micelles.[23] This appears unchanged for NCOOH/VP uptake ratios up to ca. 0.45 (noting that cross-sectional TEM showed an essentially spherical morphology in films dip-coated at 1 mm/min from equimolar solutions[22a]). Between 0.5 and equimolar, the increase in the volume fraction of the NCOOH/P4VP phase is enough to switch the morphology to cylindrical. Above equimolar, the volume fractions are such that the lamellar morphology is favored. It is noteworthy that no evidence of macroscopic phase separation, such as crystallized SM, was observed in the latter films. This is reinforced by examination of the infrared carbonyl band in the films with uptake ratios of 0.6 (VP in excess) and 1.5 (NCOOH in excess). The band is essentially identical in both films, showing a maximum at 1694 cm^{-1} compared to 1676 cm^{-1} for pure NCOOH (Figure SI-1 in the Supporting Information), where the latter is associated with crystallized H-bonded dimers. The quasi-absence of this band in the 1.5 NCOOH/VP shows that the excess NCOOH is not crystallized; instead, it is most likely molecularly dispersed in the films (though with acid dimers not excluded).

The question now arises as to why the NOH-containing films do not show the same morphology evolution as the NCOOH-containing films, as shown above for equimolar SM/VP solutions, despite the fact that they have the same SM content for any given dip-coating rate. This must somehow be related to the different hydrogen-bonding strengths of the two SMs with P4VP, which is greater for NCOOH than for NOH.[22a,29] This could, in particular, modify the degree of selectivity for the P4VP phase, although other factors such as the block interaction parameter and interfacial energies with substrate and air may also be affected differently by the two molecules. The phase selectivity can be probed by DSC analysis of blends of the small molecules with PS and P4VP homopolymers. This was reported, for example, by van Zoelen et al., who found that a small fraction of PDP is miscible with PS, estimated to be about 5 wt % based on the degree of depression of the PS glass transition temperature (T_g), thereby affecting the thin film morphology of PS−P4VP/PDP.[33]

In our case, when blended with PS, NOH leads to a significantly greater maximal T_g depression of the homopolymer than NCOOH; i.e., the T_gs of the blends reach about 50 and 70−75 °C for NOH and NCOOH, respectively, compared to 106 °C for pure PS. In parallel, as deduced from the nontransparency of the solvent-cast films, NOH phase separates from PS at higher content (starting by 20 wt %) than NCOOH (starting by 10 wt %). In contrast, the T_g depression of P4VP is identical for both SMs at any given content, and all SM/P4VP solvent-cast films are transparent (studied up to 30 wt %). This clearly indicates that NOH has greater miscibility than NCOOH with PS, such that, for a given amount of total SM in a PS−P4VP film, there is more NOH than NCOOH in the PS domains. This is likely to be further reinforced by the greater strength of the NCOOH−VP H-bond than the NOH−VP H-bond. Both effects confer greater preference of NCOOH than NOH for the P4VP domains, thus leading to greater P4VP swelling by NCOOH than by NOH (and conversely, some degree of PS swelling by NOH and less by NCOOH). This differential phase selectivity of the two SMs can rationalize (possibly with other contributing factors) why, as the SM content in the films increases with dip-coating rate, the NCOOH-containing films in Figure 1 (and Figure 5) attain sufficient swelling of the P4VP domains to favor the (horizontal) cylindrical morphology, whereas the NOH-containing films in this figure remain characterized by the spherical morphology (until the brush layer regime is attained).

Close inspection of the 993 cm^{-1} band for free P4VP in the calibration spectra (solvent-cast films) indirectly supports the conclusion from the DSC analysis. As shown in Figure 8, this band decreases with increase in SM content, as expected (while a band for H-bonded P4VP at higher wavenumbers increases in parallel; shown by the second-derivative spectra in Figure SI-2 to be located at 1007 and 1015 cm^{-1} in the NOH- and

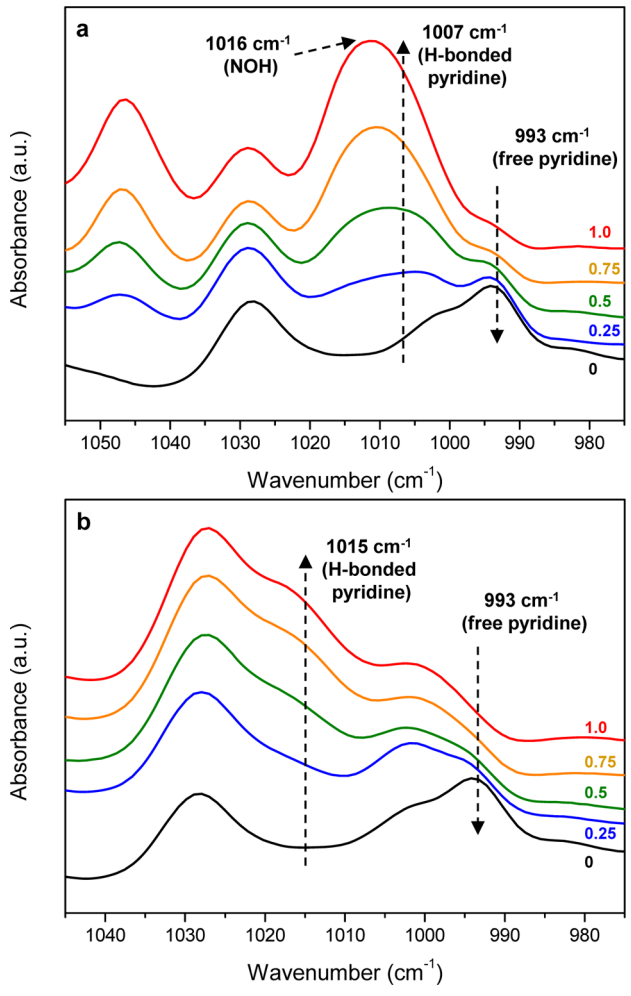

Figure 8. ATR-IR calibration spectra of the solvent-cast films of (a) PS−P4VP/NOH and (b) PS−P4VP/NCOOH at the SM/VP ratios indicated, normalized relative to the copolymer band at 1493 cm^{-1}.

dx.doi.org/10.1021/ma301383v | Macromolecules 2012, 45, 7964−7972

NCOOH-containing films, respectively). However, at equimolar ratio, it is still weakly visible in the NOH-containing, but not NCOOH-containing, films. This is consistent with a greater (but small) fraction of NOH than NCOOH being dispersed in the PS phase.

To understand the variation in uptake ratio with dip-coating rate, it is necessary to refer to the film thickness variation with this rate. As mentioned above, we observed previously that the average thickness of dip-coated block copolymer films decreases with dip-coating rate in the range investigated.[22a] ("Average" is specified because these films tend to be subject to dewetting/terracing phenomena, described in detail in ref 22a.) Figure 9 shows that this trend is followed by the films dip-coated from solutions of all of the NCOOH/VP molar ratios studied and that the film thickness is insensitive to this ratio within experimental uncertainty. This trend in film thickness at slow dip-coating rates thus appears to be a general phenomenon, which was recently reported first for phospholipid deposition on horizontal substrates[34] and then for dip-coated sol–gel films.[25,26] The latter references also show that a further increase in dip-coating rate leads to a minimum thickness (reached in our films at the highest dip-coating rates used), followed by an increase in thickness. The approximately V-shaped dependence of film thickness on dip-coating rate was explained by the combination of two competitive dip-coating regimes:[25,26] (a) the "capillarity" regime dominating the slow dip-coating side of the minimum, which is governed by capillarity feeding of the developing film as solvent evaporates, leading to thicker films as dip-coating rate decreases, and (b) the "draining" regime dominating the high dip-coating side of the minimum, which is the usual regime used for dip-coating, first described by Landau and Levich,[35] and where film thickness increases with dip-coating rate.

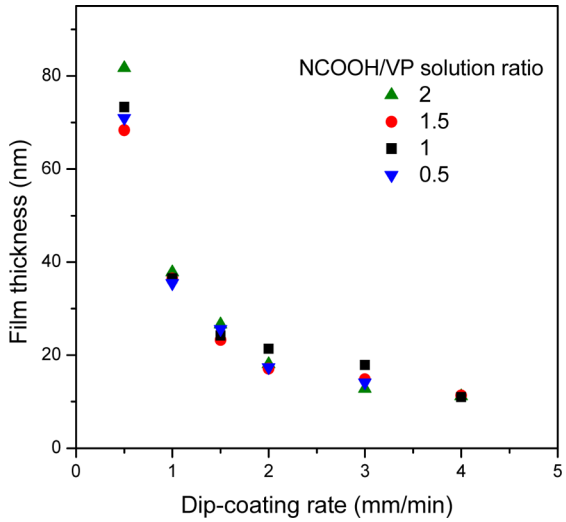

Figure 9. Average film thickness of the PS–P4VP/NCOOH films dip-coated from solutions of the NCOOH/VP molar ratios indicated.

The nature of the capillarity regime can explain the variation in SM/VP uptake ratio as follows. The very slow withdrawal of the substrate from solution in this regime allows the capillary rise (meniscus) of the solution to continuously feed the depositing film as solvent evaporates, thereby leading to increasingly thick films with decreasing substrate withdrawal rate.[25,26,34] At the same time, the lengthy contact of the meniscus with the depositing film can effectively wash out much of the small molecule from that film by diffusion back into solution, thus depleting the SM content in the final film. The slower the substrate withdrawal, the more complete the washing out of the SM. As the withdrawal rate increases, the capillarity effect decreases in importance, and therefore, the SM content in the film rises to approach that in solution, thus leading to the tendency to a plateau in the uptake ratios with dip-coating rate, as observed in Figures 5–7.

In general, the dependence of the SM/VP uptake ratio is likely to depend on the nature of the solvent. As mentioned in the Introduction, THF competes with P4VP as a hydrogen bond acceptor. This was shown by NMR in ref 24 for PDP in d-THF, where the hydroxyl proton has a high chemical shift (7.97 ppm) indicative of strong interactions with THF; this shift is unchanged (7.99 ppm) in the presence of PS–P4VP, indicating insignificant interaction of PDP with P4VP in THF. (In contrast, the shifts in d-$CHCl_3$ were measured to be 4.63 and 5.26 for PDP alone and in the presence of PS–P4VP, respectively, indicating weak interactions of PDP with this solvent and H-bonding with the P4VP block.[24]) In our systems, the shifts measured for the hydroxyl proton of NOH alone and the acid proton of NCOOH alone in d-THF are 8.91 and 11.55 ppm, respectively, compared to 8.94 and 11.59 ppm, respectively, in the presence of PS–P4VP (equimolar SM:VP), thus confirming the strong interactions of NOH and NCOOH with THF at the expense of interactions with P4VP. In other words, by the shear number of THF molecules compared to VP moieties in solution, THF effectively overwhelms SM hydrogen bonding with P4VP. This rationalizes why the hydrodynamic radius, the radius of gyration, and therefore the micelle shape and size of PS–P4VP in THF are unchanged by the presence of either SM.[22a] It can also explain why there is no difference between NOH and NCOOH in uptake ratio and its trend with dip-coating rate (Figure 5). In addition, these effects may mediate the distributions of NOH vs NCOOH between the PS and P4VP domains discussed above. Specifically, as the THF evaporates from the deposited film, the SM will tend to migrate to the P4VP domains, probably more strongly (or at higher THF content) for the stronger hydrogen-bonding SM, NCOOH. On the other hand, if a solvent that is less competing or noncompeting for the H-bond is used, the SM binds partly or completely (up to stoichiometrically) with the P4VP in solution,[24] to thus be less prone or not at all prone to washing out during the dip-coating process. Preliminary results using $CHCl_3$, which is currently under investigation (along with other solvents), indeed suggest that this is the case.

It is of interest to compare the above results with related observations by Stamm and co-workers, particularly regarding their extensive work with dip-coated HABA-containing PS–P4VP films. It is first important to point out that their films were dip-coated in the draining regime (0.1–1.0 mm/s), although, to our knowledge, they did not investigate the effect of dip-coating rate specifically.[5,11−13,16−18,36] Since the uptake ratio in Figures 5–7 tends toward the SM/VP solution ratio as the minimum film thickness is approached, it can be surmised that the film composition in the draining regime, where the capillarity effect ceases, is the same as in solution. We have indeed confirmed this by extending our investigations to higher dip-coating rates, as reported elsewhere.[23] With this in mind, it is notable that Nandan et al. observed that increasing the SM/VP molar ratio in dioxane solution transforms a spherical morphology to in-plane cylindrical morphology in dip-coated films, due to greater swelling of the P4VP domains by the

dx.doi.org/10.1021/ma301383v | Macromolecules 2012, 45, 7964–7972

increased SM content.[18] This is identical to what is observed in Figure 6 below and above line A for increasing SM/VP solution ratio at dip-coating rates between 1 and 3 mm/min. Furthermore, the effect of the capillarity regime on the SM uptake in the films allows this effect to occur simply by varying the dip-coating rate from a single dip-coating solution composition.

The above results highlight the importance of determining the SM content and its evolution with dip-coating rate, in conjunction with film thickness and other effects, in understanding morphology evolution in supramolecular dip-coated films, particularly in the capillarity regime of dip-coating rates. Block fraction composition and film thickness relative to the bulk periodicity are known from annealed spin-coated films to be two important factors governing thin film morphology and orientation.[10] Other factors include the solvent used,[16] its interactions with either or both blocks and consequent modification of block−block and block−SM interactions,[20,37] its evaporation rate,[38] and solution concentration.[22a,27] Typically, kinetic factors, and thus the pathway taken in the phase diagram as solvent evaporates, also play a significant role.[11] Several of these effects have been shown and discussed in the work of Stamm and co-workers[5,11−13,16−18,36] as well as by ten Brinke and co-workers[19,20,33] for supramolecular films. Finally, it should be emphasized that the dip-coated films described here are not postannealed, in contrast to most investigations of spin-coated films, which are generally thermally or solvent annealed to reveal morphologies.

CONCLUSIONS

We have shown that the morphology of self-assembling films dip-coated slowly from THF solutions of PS−P4VP block copolymers mixed with NOH and NCOOH depend on the nature of the hydrogen-bonding small molecule (such as its H-bond strength) and, at least for NCOOH, on the SM/VP ratio in the film. In turn, the SM/VP ratio in the film, determined by ATR-IR spectroscopy, is proportional to the ratio in solution with the proportionality increasing toward unity with dip-coating rate, this in the same way for both NOH and NCOOH. The latter dependence is related to the dip-coating taking place in the so-called capillarity regime, where the film thickness is governed by capillarity feeding.[25,26] In this regime, the slower the dip-coating rate, the thicker the film and, simultaneously, the more time there is for diffusion of the small molecule (NOH or NCOOH here) back into solution, thereby decreasing its amount in the final film. This diffusion effect is considered to be effective when using H-bond competing solvents (here THF). For lower SM content, the morphology is essentially spherical due to the spherical micellar nature of the block copolymer in solution. For NCOOH, the morphology evolves to (in-plane) cylindrical and then lamellar with increasing NCOOH content (higher dip-coating rates), which is explained by the increased selective swelling of the P4VP domains in the film. NOH-containing films dip-coated from equimolar SM:VP solutions show only spherical morphology in the range studied (compared to spherical and cylindrical for NCOOH-containing films in the same range). This is attributed to greater miscibility of NOH than NCOOH with PS (supported by thermal studies of the glass transition temperature depression), such that the P4VP/NOH domains do not attain the necessary volume fraction for the development of cylindrical morphology.

ASSOCIATED CONTENT

Supporting Information

Comparison of infrared spectra in the carbonyl region and of second-derivative spectra in the 1000 cm^{-1} region. This material is available free of charge via the Internet at http://pubs.acs.org.

AUTHOR INFORMATION

Corresponding Author

*E-mail: c.pellerin@umontreal.ca (C.P.); geraldine.bazuin@umontreal.ca (C.G.B.); re.prudhomme@umontreal.ca (R.E.P.).

Notes

The authors declare no competing financial interest.

ACKNOWLEDGMENTS

The research was funded by the Natural Sciences and Engineering Research Council (NSERC) of Canada and le Fonds Québécois de la Recherche sur la Nature et les Technologies (FQRNT). The authors thank B.Sc. student, Shanon Etima, for executing the DSC experiments and Ph.D. student, Xin Wang, for the NMR measurements.

REFERENCES

(1) Kim, H.-C.; Park, S.-M.; Hinsberg, W. D. *Chem. Rev.* **2009**, *110*, 146.
(2) Haberkorn, N.; Lechmann, M. C.; Sohn, B. H.; Char, K.; Gutmann, J. S.; Theato, P. *Macromol. Rapid Commun.* **2009**, *30*, 1146.
(3) Shin, D. O.; Jeong, J.-R.; Han, T. H.; Koo, C. M.; Park, H.-J.; Lim, Y. T.; Kim, S. O. *J. Mater. Chem.* **2010**, *20*, 7241.
(4) Harrison, C.; Dagata, J. A.; Adamson, D. H. In *Developments in Block Copolymer Science and Technology*; Hamley, I. W., Ed.; John Wiley & Sons: Chichester, UK, 2004; p 295.
(5) Kuila, B. K.; Nandan, B.; Böhme, M.; Janke, A.; Stamm, M. *Chem. Commun.* **2009**, 5749.
(6) Bates, F. S.; Fredrickson, G. H. *Phys. Today* **1999**, *52*, 32.
(7) Li, M.; Coenjarts, C. A.; Ober, C. K. *Adv. Polym. Sci.* **2005**, *190*, 183.
(8) Ham, S.; Shin, C.; Kim, E.; Ryu, D. Y.; Jeong, U.; Russell, T. P.; Hawker, C. J. *Macromolecules* **2008**, *41*, 6431.
(9) Kim, S.; Nealey, P. F.; Bates, F. S. *ACS Macro Lett.* **2012**, *1*, 11.
(10) Fasolka, M. J.; Mayes, A. M. *Annu. Rev. Mater. Res.* **2001**, *31*, 323.
(11) Böhme, M.; Kuila, B.; Schlorb, H.; Nandan, B.; Stamm, M. *Phys. Status Solidi B* **2010**, *247*, 2458.
(12) Kuila, B. K.; Stamm, M. *J. Mater. Chem.* **2011**, *21*, 14127.
(13) Nandan, B.; Kuila, B. K.; Stamm, M. *Eur. Polym. J.* **2011**, *47*, 584.
(14) Laforgue, A.; Bazuin, C. G.; Prud'homme, R. E. *Macromolecules* **2006**, *39*, 6473.
(15) van Zoelen, W.; ten Brinke, G. *Soft Matter* **2009**, *5*, 1568.
(16) Sidorenko, A.; Tokarev, I.; Minko, S.; Stamm, M. *J. Am. Chem. Soc.* **2003**, *125*, 12211.
(17) Tokarev, I.; Krenek, R.; Burkov, Y.; Schmeisser, D.; Sidorenko, A.; Minko, S.; Stamm, M. *Macromolecules* **2005**, *38*, 507.
(18) Nandan, B.; Vyas, M. K.; Böhme, M.; Stamm, M. *Macromolecules* **2010**, *43*, 2463.
(19) van Zoelen, W.; Polushkin, E.; ten Brinke, G. *Macromolecules* **2008**, *41*, 8807.
(20) van Zoelen, W.; Asumaa, T.; Ruokolainen, J.; Ikkala, O.; ten Brinke, G. *Macromolecules* **2008**, *41*, 3199.
(21) Tung, S.-H.; Kalarickal, N. C.; Mays, J. W.; Xu, T. *Macromolecules* **2008**, *41*, 6453.
(22) (a) Roland, S.; Gaspard, D.; Prud'homme, R. E.; Bazuin, C. G. *Macromolecules* **2012**, *45*, 5463. (b) Laforgue, A.; Gaspard, D.; Bazuin, C. G.; Prud'homme, R. E. *Am. Chem. Soc. Polym. Prepr.* **2007**, *48*, 670.

(c) Roland, S.; Pellerin, C.; Bazuin, C. G.; Prud'homme, R. E. *Am. Chem. Soc. Polym. Prepr.* **2011**, *52*, 101.
(23) Roland, S.; Prud'homme, R. E.; Bazuin, C. G. *ACS Macro Lett.* **2012**, *1*, 973.
(24) Huang, W.-H.; Chen, P.-Y.; Tung, S.-H. *Macromolecules* **2012**, *45*, 1562.
(25) Faustini, M.; Louis, B.; Albouy, P. A.; Kuemmel, M.; Grosso, D. *J. Phys. Chem. C* **2010**, *114*, 7637.
(26) Grosso, D. *J. Mater. Chem.* **2011**, *21*, 17033.
(27) Meiners, J. C.; Ritzi, A.; Rafailovich, M. H.; Sokolov, J.; Mlynek, J.; Krausch, G. *Appl. Phys. A: Mater. Sci. Process.* **1995**, *61*, 519.
(28) Cesteros, L. C.; Isasi, J. R.; Katime, I. *Macromolecules* **1993**, *26*, 7256.
(29) (a) Lee, J. Y.; Painter, P. C.; Coleman, M. M. *Macromolecules* **1988**, *21*, 954. (b) Lee, J. Y.; Moskala, E. J.; Painter, P. C.; Coleman, M. M. *Appl. Spectrosc.* **1986**, *40*, 991. (c) Coleman, M. M.; Graf, J. F.; Painter, P. C. *Specific Interactions and the Miscibility of Polymer Blends*; CRC Press: Lancaster, PA, 1991.
(30) Liang, C. Y.; Krimm, S. *J. Polym. Sci.* **1958**, *27*, 241.
(31) Panov, V. P.; Kazarin, L. A.; Dubrovin, V. I.; Gusev, V. V.; Kirsh, Y. É. *J. Appl. Spectrosc.* **1974**, *21*, 1504.
(32) Lippincott, E. R.; O'Reilly, E. J. *J. Chem. Phys.* **1955**, *23*, 238.
(33) van Zoelen, W.; Alberda van Ekenstein, G.; Ikkala, O.; ten Brinke, G. *Macromolecules* **2006**, *39*, 6574.
(34) Le Berre, M.; Chen, Y.; Baigl, D. *Langmuir* **2009**, *25*, 2554.
(35) Landau, L.; Levich, B. *Acta Physicochim. URSS* **1942**, *17*, 42.
(36) Kuila, B. K.; Stamm, M. *Macromol. Symp.* **2011**, *303*, 85.
(37) Li, Y.; Wang, X.; Sanchez, I. C.; Johnston, K. P.; Green, P. F. *J. Phys. Chem. B* **2007**, *111*, 16.
(38) Phillip, W. A.; Hillmyer, M. A.; Cussler, E. L. *Macromolecules* **2010**, *43*, 7763.